Smooth and Time-Optimal Trajectory Planning for Industrial Manipulators along Specified Paths

D. Constantinescu E.A. Croft

e-mail: daniela@mech.ubc.ca

Industrial Automation Lab.

Dept. of Mechanical Engineering

University of British Columbia

Vancouver, BC, Canada V6T 1Z4

Abstract

This paper presents a method for determining smooth and time-optimal path constrained trajectories for robotic manipulators and investigates the performance of these trajectories both through simulations and experiments. The desired smoothness of the trajectory is imposed through limits on the actuator jerks. The third derivative of the path parameter with respect to time, the pseudo-jerk, is the controlled input. The limits on the actuator torques translate into state-dependent limits on the pseudo-acceleration. The time-optimal control objective is cast as an optimization problem by using cubic splines to parameterize the state space trajectory. The optimization problem is solved using the flexible tolerance method. The experimental results presented show that the planned smooth trajectories provide superior feasible time-optimal motion.

1 Introduction

The need for increased productivity in path-following industrial robotic applications has been commonly addressed in the literature by determining path-constrained time-optimal motions (PCTOM) while accounting for actuator torque limits[1], [2], [3]. In these formulations, the joint actuator torques are the controlled inputs and the open loop control schemes result in bang-bang or bang-singular-bang controls[1], [3], [4].

PCTOM trajectories compute the maximum velocity achievable at the robot tip while still following the prescribed path. However, implementation of PCTOM in physical manipulators has drawbacks, such as joint oscillations due to finite joint stiffness and overshoot of the nominal torque limits due to unmodelled actuator dynamics. The resultant extra strain on the robot actuators could cause them to fail frequently[5], reducing the productivity of the entire workcell.

At the trajectory planning level, a number of different techniques have been devised to address the problem of discontinuous actuator torques. A modified cost function, such as time-joint torques[2] or time-square of joint torques[6], can be used to smooth the controls and improve the tracking accuracy, at the expense of motion time.

Another way of smoothing the controls is to parameterize the path by using functions that are at least C^2 continuous, i.e., continuous in acceleration. Cubic splines used for path parameterization with time as the cost function[7] result in trajectories that have continuous joint accelerations. However, the limits on the joint variables are very conservative, since they remain constant over the entire work-space. Incorporating the actuator dynamics in this problem formulation[8] transforms the actuator voltages into the limited controlled inputs. The optimal trajectory is bang-bang in the new controls and the actuator torques are no longer limited. Also, the case of singular controls is not considered since they can be avoided by an appropriate selection of the path[3] or by convexifying the set of admissible controls[9].

In this paper, a method is presented for determining time-optimal path-constrained motions subject to actuator torque and jerk limits. The resulting trajectories will be called smooth path-constrained time-optimal motions (SPCTOM) to distinguish them from the path-constrained time-optimal motions (PCTOM), which do not consider jerk limits.

The actuator jerk limits are imposed in view of the fact that unlimited jerks can cause severe vibrations in the arm that may lead to the failure of the actuators themselves. Moreover, they are used as a means to compensate for structure flexibility and inaccuracies in the robot model. This is a desired feature in industrial applications, where the robot model is not readily available. Therefore, the benefit of the SPCTOM trajectories is that they better characterize the dynamic limitations of a robot system and, hence, are suited for direct implementation on a commercial robot using non-specialized industrial controllers.

Geometric limits on robot motion, such as obstacles and joint limits, are not addressed herein, since the motion is path-constrained. That is, only the trajectory planning problem is considered. The path is either imposed by the application itself or a time-optimal path can be determined as in [10]: under the assumption that the desired path is smooth, an initial guess is generated using splines and the optimal path is found through an unconstrained parameter optimization. The cost function is composed of the motion time along the path plus penalty terms corresponding to obstacles and joint limits.

2 Smooth Path-Constrained Time-Optimal Motions

2.1 Problem Formulation

The problem of smooth path-constrained time-optimal motion (SPCTOM) planning can be stated as follows:

$$\min_{\dot{\mathbf{T}} \in \mathbf{\Omega}} J = \int_0^{t_f} 1 dt, \tag{1}$$

subject to the manipulator dynamics:

$$\mathbf{M}(\mathbf{q})\ddot{\mathbf{q}} + \dot{\mathbf{q}}^{\mathbf{T}}\mathbf{C}(\mathbf{q})\dot{\mathbf{q}} + \mathbf{G}(\mathbf{q}) = \mathbf{T}, \tag{2}$$

the boundary conditions:

$$\mathbf{q}(0) = \mathbf{q_0} \quad ; \quad \mathbf{q}(t_f) = \mathbf{q_f} \quad ; \quad \dot{\mathbf{q}}(0) = \dot{\mathbf{q}}(t_f) = 0 \quad ; \quad \ddot{\mathbf{q}}(0) = \ddot{\mathbf{q}}(t_f) = 0, \tag{3}$$

the path constraints:

$$\mathbf{r} = \mathbf{r}(s), \tag{4}$$

the actuator torque limits:

$$\mathbf{T}_{min} \leq \mathbf{T} \leq \mathbf{T}_{max}, \tag{5}$$

and the actuator jerk limits:

$$\dot{\mathbf{T}}_{min} \leq \dot{\mathbf{T}} \leq \dot{\mathbf{T}}_{max}, \tag{6}$$

where n is the number of degrees of freedom of the manipulator. Furthermore, $\mathbf{q} \in \mathbf{R}^n$ is the vector of joint positions, $\mathbf{T} \in \mathbf{R}^n$ is the vector of actuator torques, $\dot{\mathbf{T}} \in \mathbf{R}^n$ is the vector of actuator jerks, $\mathbf{M}(\mathbf{q}) \in \mathbf{R}^{n \times n}$ is the inertia matrix of the manipulator, $\mathbf{C}(\mathbf{q}) \in \mathbf{R}^{n \times n \times n}$ is a third order tensor representing the coefficients of the centrifugal and Coriolis forces, $\mathbf{G}(\mathbf{q}) \in \mathbf{R}^n$ is the vector of gravity terms, and $\mathbf{r} \in \mathbf{R}^3$ is a C^1 continuous curve parametrized by s, which may be, for example, the arc length. To simplify the dynamics, viscous and static friction terms have been neglected. However, as shown in the experiments in Section 5, the imposition of suitable actuator jerk limits compensates for these and other model inaccuracies.

In the above formulation, the actuator jerks represent the bounded controls. Since the Lagrangian form of the robot dynamics incorporates only the actuator torques, the third order dynamics is required. Differentiation of (2) with respect to time results in:

$$\mathbf{M}(\mathbf{q})\dddot{\mathbf{q}} + \dot{\mathbf{M}}(\mathbf{q})\ddot{\mathbf{q}} + \ddot{\mathbf{q}}^{\mathbf{T}}\mathbf{C}(\mathbf{q})\dot{\mathbf{q}} + \dot{\mathbf{q}}^{\mathbf{T}}\dot{\mathbf{C}}(\mathbf{q})\dot{\mathbf{q}} + \dot{\mathbf{q}}^{\mathbf{T}}\mathbf{C}(\mathbf{q})\ddot{\mathbf{q}} + \dot{\mathbf{G}}(\mathbf{q}) = \dot{\mathbf{T}}. \tag{7}$$

Equation (7) is taken as the dynamics of the system, with $\dot{\mathbf{T}}$ representing the n-dimensional bounded controls.

2.2 Path Constraints

The dynamic system described by Equation (7) has $3n$ degrees of freedom. However, the path constraints (4) parameterize the end-effector tip position by a single parameter s, reducing the order of the system to 3.

To obtain the actuator jerk bounds for the reduced order system, the joint jerk is computed as:

$$\dddot{\mathbf{q}} = \mathbf{q}'''\dot{s}^3 + 3 \cdot \mathbf{q}'' \cdot \dot{s}\ddot{s} + \mathbf{q}'\dddot{s}, \tag{8}$$

where:

$$\mathbf{q}''' = \mathbf{J}^{-1} \cdot (\mathbf{r}''' - \frac{d^2\mathbf{J}}{ds^2} \cdot \mathbf{q}' - 2 \cdot \frac{d\mathbf{J}}{ds} \cdot \mathbf{q}''), \tag{9}$$

$$\mathbf{r}''' = \frac{d^2\mathbf{J}}{ds^2} \cdot \mathbf{q}' + 2 \cdot \frac{d\mathbf{J}}{ds} \cdot \mathbf{q}'' + \mathbf{J} \cdot \mathbf{q}''', \tag{10}$$

with $\mathbf{r}$ being the end-effector position and orientation, $\mathbf{J}$ being the Jacobian of the forward kinematics map, and $'$ denoting the derivative with respect to the path parameter. Substituting Equations (7) and (8) into Equation (6) yields:

$$\dot{\mathbf{T}}_{min} \leq \mathbf{a}(s) \cdot \dddot{s} + \mathbf{b}(s) \cdot \dot{s} \cdot \ddot{s} + \mathbf{c}(s) \cdot \dot{s}^3 + \mathbf{d}(s) \cdot \dot{s} \leq \dot{\mathbf{T}}_{max}, \tag{11}$$

where:

$$\mathbf{a}_{n\times 1}(s) = \mathbf{M} \cdot \mathbf{q}', \tag{12}$$

$$\mathbf{b}_{n\times 1}(s) = 3 \cdot \mathbf{M} \cdot \mathbf{q}'' + \frac{d\mathbf{M}}{ds} \cdot \mathbf{q}' + 2 \cdot \mathbf{q}'^T \cdot \mathbf{C} \cdot \mathbf{q}', \tag{13}$$

$$\mathbf{c}_{n\times 1}(s) = \mathbf{M} \cdot \mathbf{q}''' + \frac{d\mathbf{M}}{ds} \cdot \mathbf{q}'' + \mathbf{q}''^T \cdot \mathbf{C} \cdot \mathbf{q}' + \mathbf{q}'^T \cdot \frac{d\mathbf{C}}{ds} \cdot \mathbf{q}' + \mathbf{q}'^T \cdot \mathbf{C} \cdot \mathbf{q}'', \tag{14}$$

$$\mathbf{d}_{n\times 1}(s) = \frac{d\mathbf{G}}{ds} \cdot \dot{s}. \tag{15}$$

The matrices $\frac{d\mathbf{M}}{ds}$ and $\frac{d\mathbf{G}}{ds}$ and the third order tensor $\frac{d\mathbf{C}}{ds}$ are robot dependent.

As shown in the following section, the actuator jerk bounds provide constraints on the admissible states for the robot. However, the torque bounds derived in[3], [11] are still required, since as the actuator jerk bounds become very large, the torque bounds become the limiting constraint. For infinite actuator jerks, the problem returns to PCTOM.

Following [3], the actuator torque bounds for the reduced order system are obtained substituting the path constraints (4) and Equation (2) into Equation (5):

$$\mathbf{T}_{min} \leq \mathcal{A}(s) \cdot \ddot{s} + \mathcal{B}(s) \cdot \dot{s}^2 + \mathcal{C}(s) \leq \mathbf{T}_{max}, \tag{16}$$

where:

$$\mathcal{A}_{n\times 1}(s) = \mathbf{M} \cdot \mathbf{q}', \tag{17}$$

$$\mathcal{B}_{n\times 1}(s) = \mathbf{M} \cdot \mathbf{q}'' + \mathbf{q}^{'T} \cdot \mathbf{C} \cdot \mathbf{q}', \tag{18}$$

$$\mathcal{C}_{n\times 1}(s) = \mathbf{G}. \tag{19}$$

2.3 Torque Limits

As discussed in[3], for each value of the path parameter s, the actuator torque bounds (16) translate into a polygonal feasible region in the $\dot{s}^2 - \ddot{s}$ plane. Such a region is shown schematically in Figure 1 for a 3-dof manipulator. Analytically, the actuator torque bounds translate into limits on the pseudo-velocity and the pseudo-acceleration:

$$\dot{s} \leq \dot{s}_{max,T}(s) \tag{20}$$

$$\ddot{s}_{min,T}(s, \dot{s}) \leq \ddot{s} \leq \ddot{s}_{max,T}(s, \dot{s}). \tag{21}$$

The subscript T is used to discriminate the pseudo-velocity and pseudo-acceleration bounds due to the torque constraints (16) from those due to the jerk constraints (11), which will be denoted with the subscript J.

The curve $\dot{s}_{max,T}(s)$ as represented in the $s - \dot{s}$ phase plane is called the *velocity limit curve* (VLC) and it represents an upper bound for any feasible trajectory in this plane.

2.4 Jerk Limits

A similar approach can be used to determine the pseudo-velocity, pseudo-acceleration and pseudo-jerk bounds due to the actuator jerk limits. Thus, for given values of the path parameter s and pseudo-velocity $\dot{s}$, the actuator jerk bounds (11) form a polygonal feasible region in the $\dot{s} - \dddot{s}$ plane (such as the one shown schematically in Figure 2 for a 3-dof manipulator). Analytically, the actuator jerk bounds translate into limits on the pseudo-acceleration and pseudo-jerk in the $\ddot{s} - \dddot{s}$ plane:

$$\ddot{s}_{min,J}(s, \dot{s}) \leq \ddot{s} \leq \ddot{s}_{max,J}(s, \dot{s}) \tag{22}$$

$$\dddot{s}_{min}(s, \dot{s}, \ddot{s}) \leq \dddot{s} \leq \dddot{s}_{max}(s, \dot{s}, \ddot{s}) \tag{23}$$

and a constraint on the pseudo-velocity in the $\dot{s} - \ddot{s} - \dddot{s}$ space:

$$\dot{s} \leq \dot{s}_{max,J}(s), \tag{24}$$

where $\dot{s}_{max,J}(s)$ is defined as the pseudo-velocity value for which the admissible region in the $\ddot{s} - \dddot{s}$ plane reduces to a point:

$$\ddot{s}_{min,J}(s, \dot{s}_{max,J}) = \ddot{s}_{max,J}(s, \dot{s}_{max,J}). \tag{25}$$

2.5 Admissible States

In the formulation of the SPCTOM problem proposed herein, the actuator jerk limits are imposed as a means for adjusting the smoothness of the trajectory. Hence, they are independent of the actuator torque limits. This independence is reflected in the state space, as shown in Figure 3. In this figure, the actuator torque and jerk constraints for the first three joints of the SCORBOT ER VII robot (Figure 6, Table I) are plotted together in state space for the three example actuator jerk limits in Table II.

This independence of the actuator torque and jerk limits is reflected in a new constraint on the pseudo-velocity:

$$\dot{s} \leq \min\left\{\dot{s}_{max,T}(s), \dot{s}_{max,J}(s)\right\}, \tag{26}$$

and a new constraint on the pseudo-acceleration:

$$\max\{\ddot{s}_{min,T}(s), \ddot{s}_{min,J}(s)\} \leq \ddot{s} \leq \min\{\ddot{s}_{max,T}(s), \ddot{s}_{max,J}(s)\}. \tag{27}$$

Equation 26 defines a global velocity limit curve, called the *smooth motion velocity limit curve* (SMVLC). In the $s - \dot{s}$ plane, the SMVLC is an upper bound on any feasible trajectory. The SMVLC can be computed at each point along the path by a line search using bisection (the searched domain is limited from zero to $\dot{s}_{max,T}(s)$).

The SMVLC corresponding to the three examples in Table II are plotted in Figure 4. As shown in this figure, the SMVLC is determined by a combination of both actuator torque and jerk limits. Depending on the restrictions of the jerk limits, they can determine the

SMVLC almost entirely, as shown in the third example, or they can have little influence on it, as shown in the first example.

2.6 System Dynamics

The states of the reduced system are $\mathbf{x} = (s \quad \dot{s} \quad \ddot{s})^T$, while $\dddot{s}$ is the scalar control u. The SPCTOM planning problem is reformulated as:

$$\min_u J = \int_0^{t_f} 1dt, \tag{28}$$

subject to the system dynamics:

$$\dot{\mathbf{x}} = \mathbf{f}(\mathbf{x}, u) = [x_2 \quad x_3 \quad u]^T, \tag{29}$$

the boundary conditions:

$$\begin{aligned} \mathbf{x}_0 &= (s_0 \quad \dot{s}_0 \quad \ddot{s}_0)^T \\ \mathbf{x}_f &= (s_f \quad \dot{s}_f \quad \ddot{s}_f)^T, \end{aligned} \tag{30}$$

the state inequality constraints (26) and (27), and the state-dependent control inequality constraints (23).

This reformulation shows that the SPCTOM problem is a time-optimal control (TOC) problem for a first order linear system with nonlinear state and control inequality constraints and preimposed initial and final states. Moreover, Equations (23), (26), and (27) emphasize that the state and control constraints are independently active, since the controls are limited only by the actuator jerks, while the states are limited by both the actuator jerks and the actuator torques.

3 Solution of the SPCTOM

TOC problems similar to the SPCTOM above have been solved either by applying Pontryiagin's Maximum Principle (PMP) to derive the necessary conditions for optimality and then using multiple shooting methods to solve the resulting two point boundary value problem (TPBVP)[12] or by a search for the switching points, using either dynamic programming[11] or specific algorithms[1], [2], [3].

Two difficulties arise in the application of these approaches in the present case. First, the complexity of the dynamic programming algorithms grows exponentially with the phase space dimension, rendering the method infeasible for more than two dimensions. As defined, the SPCTOM problem has a three dimensional phase space. Second, the other two approaches (based on PMP and the search for the switching points) depend on the bang-bang or bang-singular-bang structure of the optimal controls. This structure has been proven using results from Optimal Control Theory (OCT) regarding systems with state dependent control constraints[13]. However, no results have been proven using OCT concerning the necessary optimality conditions for systems with state and control constraints which are independently active. Thus, for the SPCTOM problem, it is not guaranteed that the optimal controls are bang-bang or bang-singular-bang.

To resolve these difficulties, the SPCTOM trajectory planning problem is analyzed and solved herein in the s-$\dot{s}$ phase plane. The motivation is that in this plane both trajectory end-points are fixed, while in the time domain the final point is free. Thus, the TOC problem lends itself to a nonlinear parameter optimization in this phase plane. The motion time is computed as:

$$t(s) = \int_{s_0}^{s_f} \frac{ds}{\dot{s}}, \tag{31}$$

where s_0 and s_f are the initial and the final values of the path parameter, respectively. Therefore, the SPCTOM in the s-$\dot{s}$ phase plane is the smooth curve that minimizes $t(s)$ over the curve while not violating actuator torque and/or actuator jerk limits.

In view of the above, the optimal motion is determined by an optimization of a base trajectory. A set of cubic splines with preselected knot-point locations are chosen as the base trajectory for the optimization. Cubic polynomials have been selected to approximate the SPCTOM because they are the lowest degree polynomials that result in a smooth curve, i.e., continuous and differentiable everywhere. The location of the knots along the path have been chosen to be the same as the location of the switching points of the PCTOM (Figure 5). Since the PCTOM represents the limit for SPCTOM, these switching points are, in the limit, the same for SPCTOM and provide a reasonable estimate for the location of the SPCTOM switching points along the parameterized path.

Extra knot points could be chosen; however, the number of the PCTOM trajectory switching points could be high and the addition of extra knots would significantly increase the number of optimization variables. Therefore, extra knots will be inserted only when the corresponding PCTOM trajectory has one single switching point, because in this case the trajectory parameterization by only two splines is potentially inadequate.

This conjecture is supported by simulations which have shown that doubling the number of knots improves the SPCTOM motion time with 3-6% for five switching points and with 10-17% for one switching point, with a larger decrease in motion time for trajectories with larger jerks[14].

The variables of the optimization are the end-effector pseudo-velocities at the preselected knot-points along the path and the slopes of the trajectory in the s-$\dot{s}$ phase plane at the path end-points. These variables control the motion time: the higher the knot-points over the whole trajectory (as located in the phase plane), the shorter the motion time. On the other hand, the end slopes control the speed at which the actuator torques leave or approach their static equilibrium values. Therefore, steeper slopes also result in faster motion.

Thus, the vector of optimization variables, $\mathbf{x}$, is defined as the following parameter set:

$$\mathbf{x} = \begin{pmatrix} \frac{\left(\frac{d\dot{s}}{ds}\right)_0}{\left(\frac{d\dot{s}}{ds}\right)_{m,0}} & \frac{\dot{s}_1}{\dot{s}_{m,1}} & \cdots & \frac{\dot{s}_p}{\dot{s}_{m,p}} & \frac{\left(\frac{d\dot{s}}{ds}\right)_f}{\left(\frac{d\dot{s}}{ds}\right)_{m,f}} \end{pmatrix}^T, \tag{32}$$

where the values with the index m correspond to the limiting PCTOM (the dotted line in Figure 5), while the other values correspond to the splined trajectory (the solid line). These variables are normalized since the end slopes vary over a much wider range than the pseudo-velocities.

The optimal trajectory results from splining cubic polynomials in the s-$\dot{s}$ phase plane based on the optimized parameters $\mathbf{x}^*$. The trajectory must be within actuator torque and actuator jerk limits and take minimum time. The actuator torque and jerk constraints in

Equations (16) and (11) thus become:

$$g_{4(i-1)+1}(\mathbf{x}) = 1 - \max_{\dot{s}(s)} \frac{T_i}{T_{max,i}}, \tag{33}$$

$$g_{4(i-1)+2}(\mathbf{x}) = 1 - \max_{\dot{s}(s)} \frac{T_i}{T_{min,i}}, \tag{34}$$

$$g_{4(i-1)+3}(\mathbf{x}) = 1 - \max_{\dot{s}(s)} \frac{\dot{T}_i}{\dot{T}_{max,i}}, \tag{35}$$

$$g_{4(i-1)+4}(\mathbf{x}) = 1 - \max_{\dot{s}(s)} \frac{\dot{T}_i}{\dot{T}_{min,i}}, \tag{36}$$

for $i = 1 \ldots n$. By this definition, whenever any of the actuator torques and/or jerks exceeds its limits, the respective constraint becomes negative.

As formulated, the optimization is solved using the flexible tolerance method (FTM)[15]. There are two reasons for choosing this method. First, the derivatives of the constraints and the cost function, i.e., motion time, are not available. Second, the FTM keeps the search close to the boundary of the admissible region and can find a minimum that lies exactly on the boundary. The details of the FTM are discussed in the Appendix A.

4 Simulations

The method for determining optimal SPCTOM has been implemented in MATLAB[16] and simulations are performed considering only the positional dof of the SCORBOT ER VII robot in the Industrial Automation Laboratory at UBC (Figure 6). Thus, for the simulations performed here, the robot is an elbow manipulator with the DH parameters and the estimated masses and inertias given in Table I.

The actuator torque limits are the same for all the three examples given in this paper, while the limits on the jerks are different, as successively shown in Table II.

4.1 Planning Performance

To determine the influence of the trajectory smoothness on the motion time, a straight line in the robot work space is chosen as the preimposed path. In parametric form, the path is given as:

$$
\begin{aligned}
x(s) &= 0.4 \\
y(s) &= 0.3s - 0.1 \\
z(s) &= 0.2s + 0.3 \qquad (37)\\
s &= 0, \ldots, 1.
\end{aligned}
$$

The resulting optimal trajectories for the different limits on the actuator jerks are shown in Figures 7, 8 and 9, respectively, by solid lines. The dashed lines represent the time-optimal trajectory considering only torque limits (PCTOM). The dotted lines are the smooth motion velocity limit curves (SMVLC), i.e., the velocity limit curves determined considering both torque and jerk limits. The corresponding actuator torques and jerks are also plotted in these figures.

While the PCTOM takes 0.59 seconds, the SPCTOM takes 0.7 seconds in the first example. Here, the limits on the actuator jerks were very high and the trajectory is determined by the limits on the actuator torques. In the ideal case, both trajectories should yield same motion times; however, there are two reasons for the increase in motion time for SPCTOM : (i) the limited parameterization chosen in the $s - \dot{s}$ phase plane and (ii) the significant decrease in peak actuator jerks for SPCTOM (solid lines) compared to PCTOM (dotted lines), as shown in the semi-log-scale plot in Figure 10.

In examples 2 and 3, the limits on the actuator jerks predominate. Therefore, the torque constraints are not approached. The optimal motion times for these examples are higher, 0.735 seconds and 1.5 seconds, respectively.

The optimal trajectories determined through the proposed method are not bang-bang in the controls. This is a consequence of the parameterization in the phase plane. However, as seen from the first example presented, the chosen parameterization alone causes a comparatively small increase in the motion time.

As expected, the more restrictive the limits on actuator jerks are, the higher the motion time is. The planning simulations, however, give no indication of the relationship between trajectory smoothness and the tracking performance of the controller. To establish tracking performance five simulations, followed by five experiments were performed.

4.2 Tracking Performance

The three SPCTOM trajectories computed above, together with the PCTOM trajectory and an optimized quintic polynomial trajectory have been implemented on a simulated model of the SCORBOT ER VII robot with friction under computed torque (CT) control.

Both the robot model and the controller have been built in the MATLAB Simulink Toolbox[17]. Friction has been modeled as Coulomb and viscous friction, with the Coulomb friction coefficients 2.0Nm and the viscous friction coefficients 0.2Nmsec for all three links. The controller has been tuned for critical damping and a rise time of 200[msec] for a sampling frequency of 200Hz. In the simulations, the actuator torques saturate at 10Nm, which is the torque limit considered during planning.

The tracking performance of the CT controller for all five trajectories is plotted in Figure 11, while the planned and simulated actuator torques are plotted in Figures 12-16. The results are summarized in Table III.

As seen in Figure 11, due to actuator torque saturation, the controller cannot keep the end-effector on the path when the actuator jerks are too high. *This is the case with the PCTOM trajectory and the SPCTOM trajectory corresponding to actuator jerk limits of* 1000*Nm/sec (labeled 'spctom1' in Figure 11). This result shows that actuator jerk limits are extremely important for the ability of the system to track a planned trajectory, especially given inaccurately identified or modelled system dynamics. As expected, the smoother the trajectory, i.e., the lower the actuator jerk limits, the higher the tracking accuracy of the controller. For the PCTOM and SPCTOM with high jerk limits trajectories, the simulation predicts actuator saturation, which results not only in decreased tracking performance, but also in longer motion time (Table III).*

For the same actuator jerk limits, the simulations show similar tracking performance for the SPCTOM and the quintic trajectories. However, the SPCTOM trajectory takes 1.5sec, compared to 2sec for the quintic trajectory.

5 Experiments

All the above trajectories have also been implemented on the SCORBOT ER VII in the IAL at UBC. The robot is controlled by a TMS320C32 DSP board, interfaced with two axis control cards, each capable of handling three axes simultaneously. An open architecture real-time operating system (ORTS)[18] is used in the implementation of the control algorithm and in reading the pre-planned trajectories and feeding them to the control loop at the controller frequency. The axis control cards and the real-time operating system ORTS were developed by the Manufacturing Automation Laboratory, UBC. For the purpose of the experiments reported here, only the positional degrees of freedom of the robot are considered, thus the robot is treated as a 3-dof elbow manipulator with the kinematic and dynamic parameters given in Table I. *Trajectory tracking is ensured by a tuned computed torque controller. While not typical in industry, such a controller allows the experiments to reflect the influence of the planned trajectory on the system performance.*

The results of the experiments are plotted in Figures 17-21, and summarized in Table IV.

These experimental results support the simulation results. Namely, for high actuator jerk limits, the controller cannot keep the end-effector on the path. Figures 17, 18, and 19 show that trajectories with high jerks result in increased tracking errors, which, in turn, activate the controller, saturating the actuators. Whenever this happens, the end-effector leaves the path. Such a trajectory is an infeasible trajectory. For the case of the SCORBOT ER VII manipulator, actuator jerk limits less than one order of magnitude higher than the actuator torque limits are required to ensure that the end-effector follows the planned path. While this result is more restrictive for the jerk limits than predicted by the simulations, it is not totally unexpected. Due to the large errors involved in modelling the system, one would expect that the simulation results would overestimate the system capabilities.

The experimental performance of the SPCTOM trajectory corresponding to the low jerk limits, i.e. 10Nm/sec, is similar to its simulated performance. Thus, while being tracked by the controller with similar accuracy and effort as the quintic trajectory, it results in reduced motion time (1.5sec compared to 2sec). This indicates that actuator jerk limits are preferable when determining smooth time optimal motions over global velocity and acceleration limits.

6 Conclusions

A method has been presented for determining smooth and time-optimal path-constrained trajectories for robotic manipulators. The dynamics of the manipulator together with limits on the actuator torques and jerks are considered. A base trajectory is constructed in the $s - \dot{s}$ phase plane using parameterized cubic splines and a set of initial, final, and knot point conditions derived from PCTOM without actuator jerk limits. Thus, the optimal motion is obtained through an optimization of this base trajectory, subject to actuator and jerk limits.

In planning simulations, the trajectory smoothness has a negative impact on the motion time, lower jerk limits resulting in higher motion time. However, both controller simulations and experiments have shown that, in practice, trajectory smoothness has a positive effect on both the tracking performance of the controller and the actual motion time. Moreover, a smoothly planned trajectory can compensate for a poorly modeled robot system, which is often the case in industrial practice.

Compared to a quintic polynomial trajectory with velocity and acceleration limits, the SPCTOM trajectory results in a faster motion for similar tracking performance. Thus, actuator jerk limits are preferable when imposing a desired degree of trajectory smoothness over quintic polynomials, since they are not posture-dependent.

A Appendix

In the flexible tolerance method (FTM)[15], the optimization problem:

$$\text{Minimize:} \quad f(\mathbf{x}) \quad \mathbf{x} \in \mathbf{R}^n \tag{A.1}$$

$$\text{Subject to constraints:} \quad h_i(\mathbf{x}) = 0 \quad i = 1, ..., m \tag{A.2}$$

$$g_i(\mathbf{x}) \geq 0 \quad i = m+1, ..., p$$

is solved as the following simpler equivalent problem with only one constraint:

$$\text{min:} \quad f(\mathbf{x}) \quad \mathbf{x} \in \mathbf{R}^n \tag{A.3}$$

$$\text{subject to:} \quad \Phi^{(k)} - \mathcal{T}(\mathbf{x}) \geq 0.$$

$\Phi^{(k)}$ is the value of the flexible tolerance criterion at the kth step of the optimization and it also serves as a criterion for the termination of the search, and $\mathcal{T}$ is a positive functional of all the equality and/or inequality constraints of the original problem. The cost function $f(\mathbf{x})$ and the equality and inequality constraints in (A.3) may be linear and/or non-linear functions of the variables in $\mathbf{x}$. The value of the cost function is improved by using information provided by feasible points, as well as certain nonfeasible points called *near-feasible points*. The near-feasibility limits are made more restrictive as the search advances, until in the limit only feasible points are accepted.

In (A.4) below, $\mathcal{T}(\mathbf{x})$ is used as a measure of the constraint violation, while Φ is selected as a positive decreasing function of the $\mathbf{x}$ points in $\mathbf{R}^n$. For the SPCTOM:

$$\mathcal{T}(\mathbf{x}) = \begin{cases} \max_i g_i(\mathbf{x}) & \text{if} \quad \exists_i \quad \text{such that} \quad g_i(\mathbf{x}) \geq 1 \\ 0 & \text{otherwise,} \end{cases} \tag{A.4}$$

and:

$$\Phi^{(k)} = \min\{\Phi^{(k-1)}; \kappa \sum_{i=1}^{r+1} \|x_i^{(k)} - x_{centr}^{(k)}\|\} \tag{A.5}$$

with κ a constant.

The tolerance criterion is used to classify points in $\mathbf{R}^n$. At the kth step of the optimization, a point $\mathbf{x}^{(k)}$ is said to be:

1. Feasible, if $\mathcal{T}(\mathbf{x}) = 0$
2. Near-feasible, if $0 \leq \mathcal{T}(\mathbf{x}) \leq \Phi^{(k)}$
3. Nonfeasible, if $\mathcal{T}(\mathbf{x}) < \Phi^{(k)}$.

A small value of $\mathcal{T}(\mathbf{x}^{(k)})$ implies that $\mathbf{x}^{(k)}$ is relatively near to the feasible region, and a large value of $\mathcal{T}(\mathbf{x}^{(k)})$ implies that $\mathbf{x}^{(k)}$ is relatively far from the feasible region.

On a transition from $\mathbf{x}^{(k)}$ to $\mathbf{x}^{(k+1)}$, the move is said to be feasible if $0 \leq \mathcal{T}(\mathbf{x}^{(k+1)}) \leq \Phi^{(k)}$, and nonfeasible if $\Phi^{(k)} \leq \mathcal{T}(\mathbf{x}^{(k+1)})$.

The FTM entails two independent optimizations : an outer minimization of the cost function $f(\mathbf{x})$ and an inner minimization of the violation of constraints $\mathcal{T}(\mathbf{x})$ whenever the minimization of $f(\mathbf{x})$ yields an infeasible point. The outer optimization of the motion time is implemented in this paper using the flexible polyhedron method (FPM)[19]. The FPM is a search in n dimensions where the polyhedron changes shape to match the changing shape of the surface. In the vicinity of a minimum the polyhedron shrinks, surrounding the minimum. Replacement of an infeasible point with a feasible or near feasible one is done through a line search using interval halving.

Acknowledgements

This work has been supported by the National Sciences and Engineering Research Council of Canada and the Faculty of Graduate Studies at UBC. The helpful suggestions of Professor B. Benhabib of the Department of Mechanical and Industrial Engineering of the University of Toronto is greatly appreciated. Also, the assistance of Professor Y. Altintas and the graduate students in the MAL, UBC, during the experimental part of this work is greatfully acknowledged.

References

[1] J.E. Bobrow, S. Dubowsky, and GibsonJ.S. Time-Optimal Control of Robotic Manipulators Along Specified Paths. *International Journal of Robotics Research*, 4(3):3–17, 1985.

[2] F. Pfeiffer and R. Johanni. A Concept for Manipulator Trajectory Planning. *IEEE Journal of Robotics Automation*, RA-3(2):115–123, 1987.

[3] Z. Shiller and H.H. Lu. Computation of Path Constrained Time Optimal Motions with Dynamic Singularities. *ASME Transactions, Journal of Dynamic Systems, Measure-*

ment, and Control, 114(1):34–40, March 1992.

[4] Y. Chen and A. A. Desrochers. Structure of Minimum-Time Control Law for Robotic Manipulators with Constrained Paths. In *IEEE International Conference on Robotics and Automation*, pages 971–976, Scottsdale, Arizona, 1989.

[5] J Li, R.W. Longman, V.H. Schultz, and H.G. Bock. Implementing Time Optimal Robot Maneuvers Using Realistic Actuator Constraints and Learning Control. *Astrodynamics 1998*, RA-3(2):115–123, 1987.

[6] Z. Shiller. Time-Energy Optimal Control of Articulated Systems with Geometric Path Constraints. In *IEEE International Conference on Robotics and Automation*, pages 2680–2685, San Diego, California, 1994.

[7] C.S. Lin, P.R. Chang, and J.Y.S. Luh. Formulation and Optimization of Cubic Polynomial Joint Trajectories for Industrial Robots. *IEEE Transactions on Automatic Control*, AC-28(12):1066–1074, 1983.

[8] M. Tarkiainen and Z. Shiller. Time Optimal Motions of Manipulators with Actuator Dynamics. In *IEEE International Conference on Robotics and Automation*, pages 725–730, Los Alamitos, California, 1993.

[9] Z. Shiller. On Singular Time-Optimal Control Along Specified Paths. *IEEE Transactions on Robotics and Automation*, 10(4):561–571, 1994.

[10] Z. Shiller and S Dubowsky. Time Optimal Path Planning for Robotic Manipulators with Obstacles, Actuator, Gripper, and Payload Constraints. *International Journal of Robotics Research*, 8(6):3–18, December 1989.

[11] K.G. Shin and N.D. McKay. A Dynamic Programming Aproach to Trajectory Planning of Robotic Manipulators. *IEEE Transactions on Automatic Control*, AC-31(6):491–500, June 1986.

[12] H.G. Bock and K.-J. Plitt. A Multiple Shooting Algorithm for Direct Solution of Optimal Control Problems. In *9th IFAC World Congress*, pages 1853–1858, Budapest, Hungary, 1984.

[13] G. Leitman. *The Calculus of Variations and Optimal Control.* Plenum Press-New York and London, 1981.

[14] D. Constantinescu. Smooth Time Optimal Trajectory Planning for Industrial Manipulators. Master's thesis, University of British Columbia, 1998.

[15] D.M. Himmelblau. *Applied Nonlinear Programming.* McGraw-Hill, 1989.

[16] The MathWorks, Natwik, Massachusetts. *Matlab User's Guide*, 1995.

[17] The MathWorks, Natwik, Massachusetts. *Simulink Toolbox User's Guide*, 1995.

[18] N.A. Erol and Y. Altintas. Open Architecture Modular Tool Kit for Motion and Process Control. In *ASME International Mechanical Engineering Congress and Exposition, ASME Publication MED*, pages 15–22, Dallas, Texas, 1997.

[19] J.A. Nelder and R. Mead. A Simplex Method for Function Minimization. *Computer Journal*, 4:308–313, 1964.

List of Figures

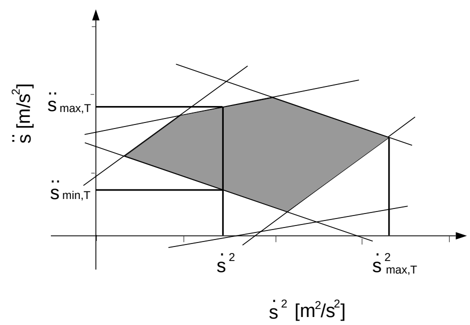

Figure 1: Admissible region in the $\dot{s}^2 - \ddot{s}$ plane, after [3].

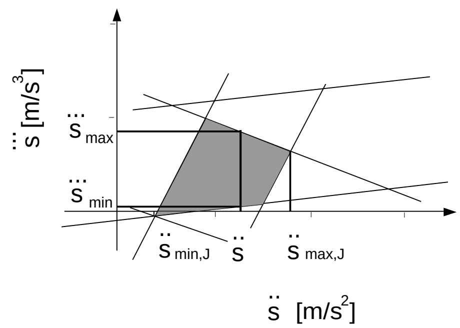

Figure 2: Admissible region in the $\ddot{s} - \dddot{s}$ plane.

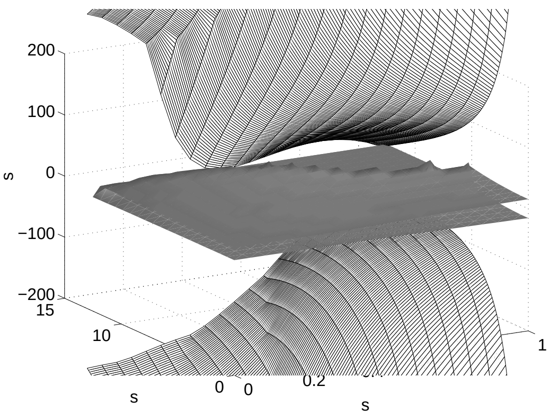

(a) Example 1 (high jerk limits): meshed surfaces - jerk limits ; shaded surfaces - torque limits.

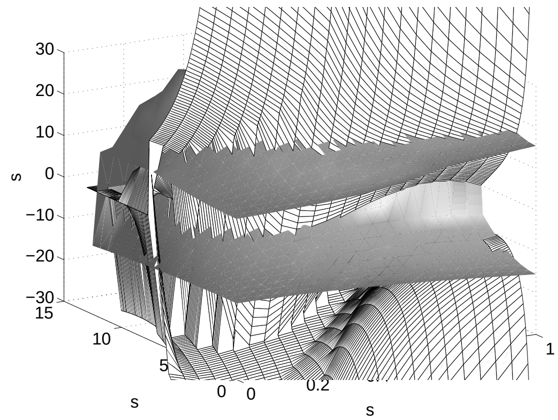

(b) Example 2 (medium jerk limits): meshed surfaces - jerk limits ; shaded surfaces - torque limits.

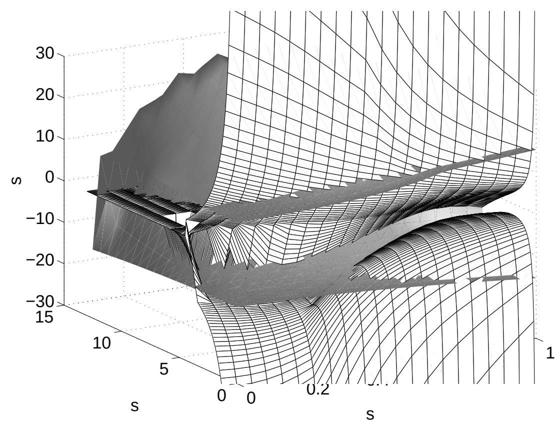

(c) Example 3 (low jerk limits): meshed surfaces - jerk limits ; shaded surfaces - torque limits.

Figure 3: Admissible states in the $s - \dot{s} - \ddot{s}$ space.

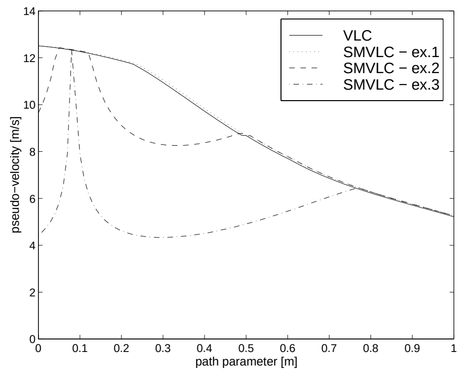

Figure 4: SMVLC for different actuator jerk limits.

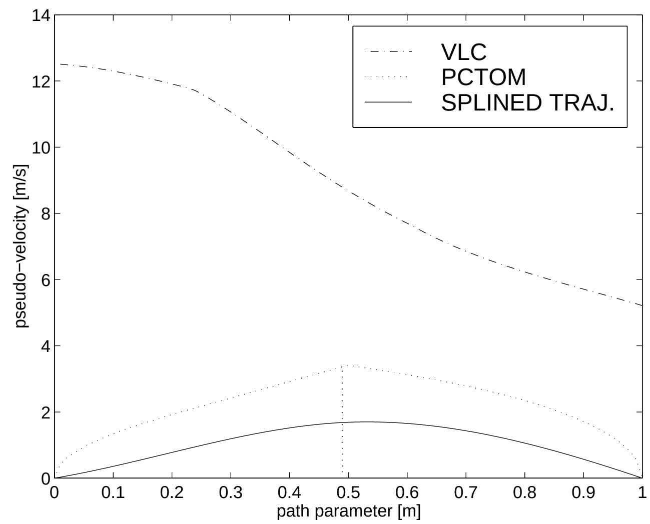

Figure 5: Switching points of the PCTOM (dotted line) and a sample splined trajectory (solid line)

Figure 6: The SCORBOT ER VII robot.

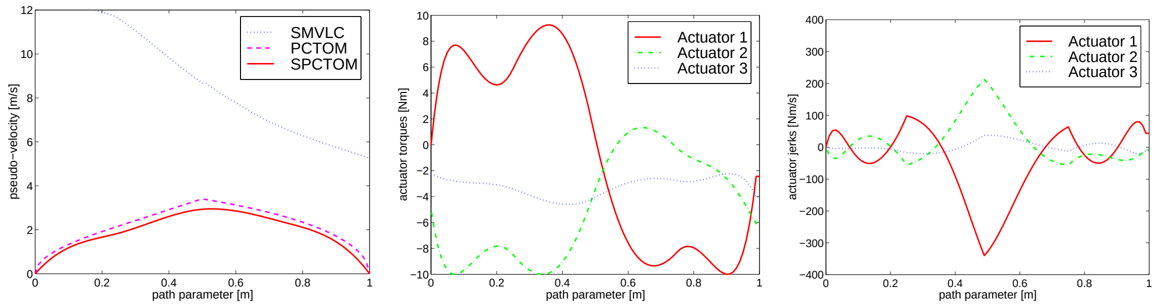

(a) SPCTOM trajectory in the $s - \dot{s}$ plane.

(b) Actuator torques.

(c) Actuator jerks.

Figure 7: Example 1 (high jerk limits).

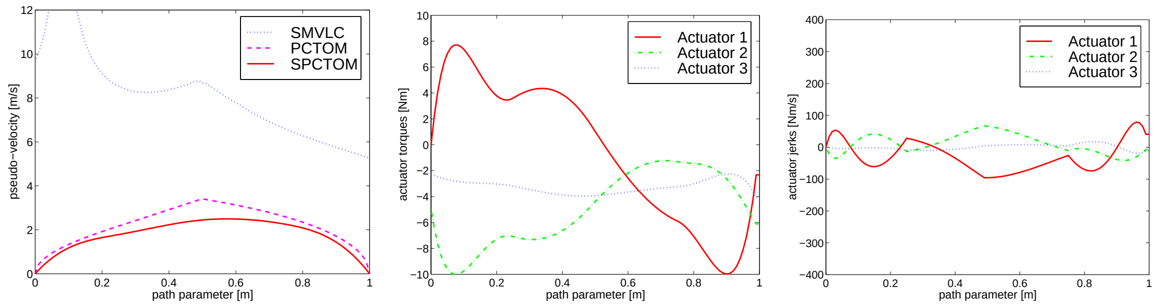

(a) SPCTOM trajectory in the $s - \dot{s}$ plane.

(b) Actuator torques.

(c) Actuator jerks.

Figure 8: Example 2 (medium jerk limits).

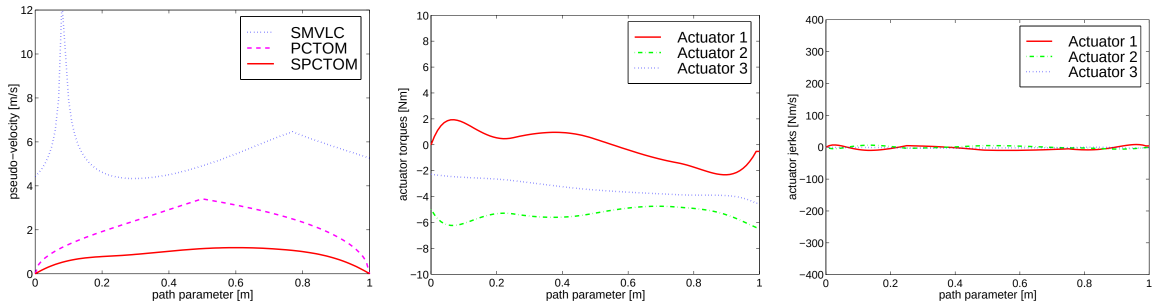

(a) SPCTOM trajectory in the $s - \dot{s}$ plane.

(b) Actuator torques.

(c) Actuator jerks.

Figure 9: Example 3 (low jerk limits).

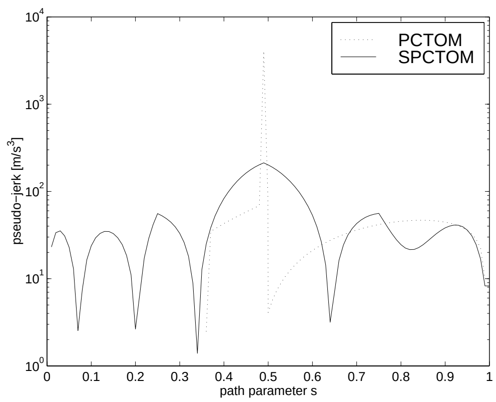

Figure 10: Absolute values of the actuator jerks for the SPCTOM in example 1 (solid lines) and PCTOM (dotted lines)

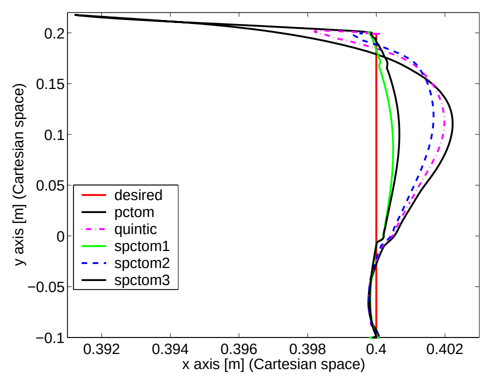

(a) Paths in the x0y plane.

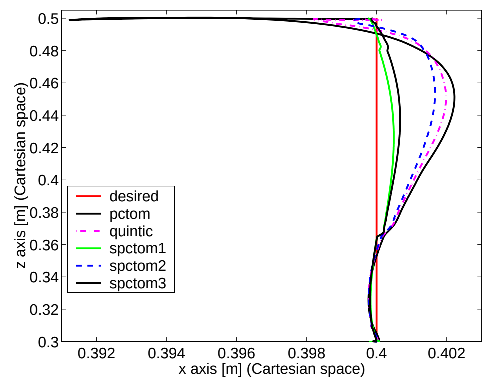

(b) Paths in the x0z plane.

Figure 11: Simulated controller tracking performance for the PCTOM, quintic, and SPCTOM trajectories.

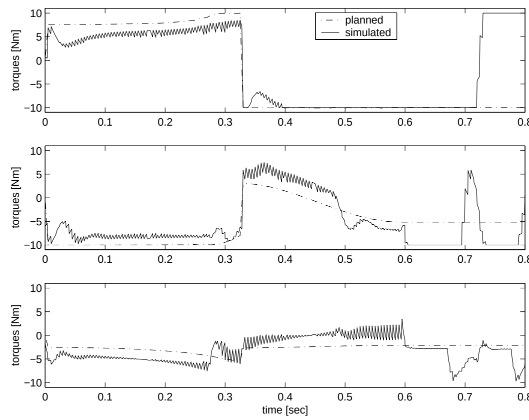

Figure 12: Desired and simulated torques for the PCTOM trajectory.

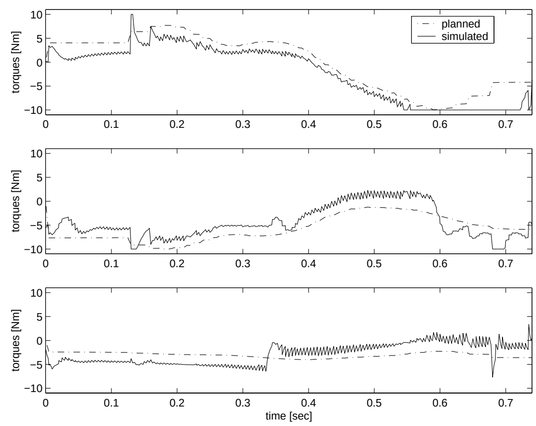

Figure 13: Desired and simulated torques for the SPCTOM trajectory (Example 1 - jerk limits of 1000Nm/sec).

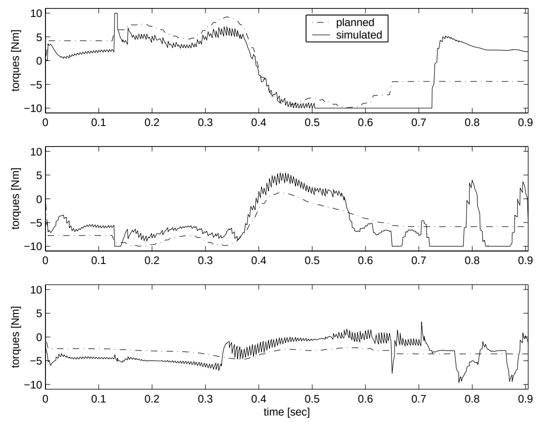

Figure 14: Desired and simulated torques for the SPCTOM trajectory (Example 2 - jerk limits of 100Nm/sec).

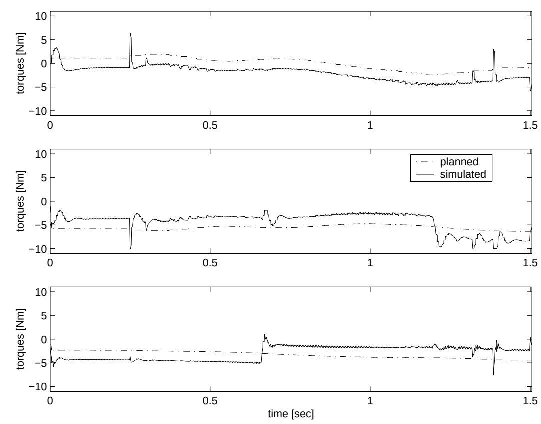

Figure 15: Desired and simulated torques for the SPCTOM trajectory (Example 3 - jerk limits of 10Nm/sec).

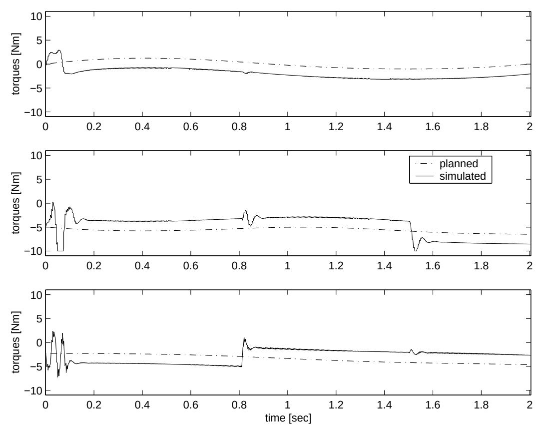

Figure 16: Desired and simulated torques for the quintic trajectory.

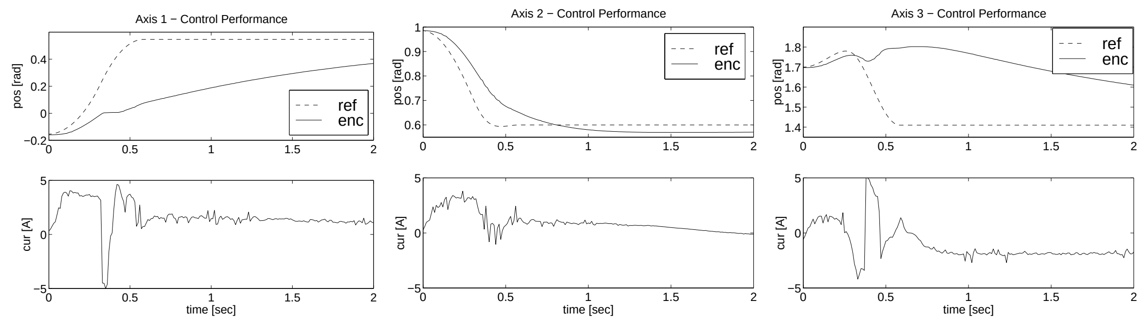

(a) Joint 1 performance (b) Joint 2 performance (c) Joint 3 performance

Figure 17: Experimental results for the PCTOM trajectory implemented on the SCORBOT ER VII.

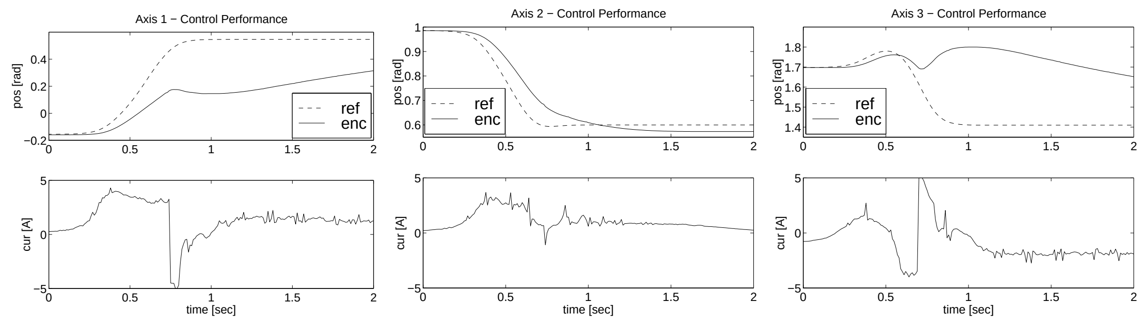

(a) Joint 1 performance (b) Joint 2 performance (c) Joint 3 performance

Figure 18: Experimental results for the SPCTOM trajectory (Example 1 - jerk limits of 1000Nm/sec) implemented on the SCORBOT ER VII.

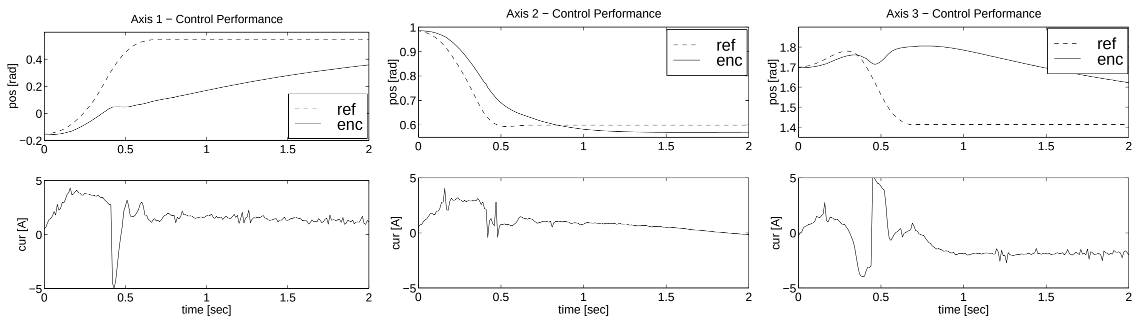

(a) Joint 1 performance (b) Joint 2 performance (c) Joint 3 performance

Figure 19: Experimental results for the SPCTOM trajectory (Example 2 - jerk limits of 100Nm/sec) implemented on the SCORBOT ER VII.

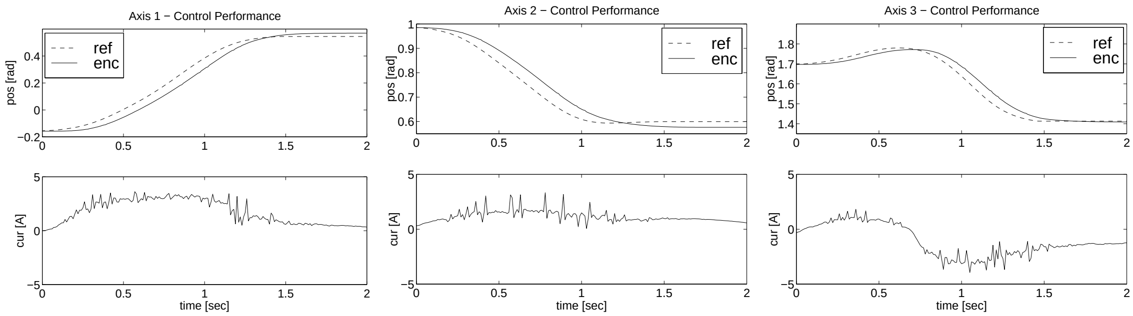

(a) Joint 1 performance (b) Joint 2 performance (c) Joint 3 performance

Figure 20: Experimental results for the SPCTOM trajectory (Example 3 - jerk limits of 10Nm/sec) implemented on the SCORBOT ER VII.

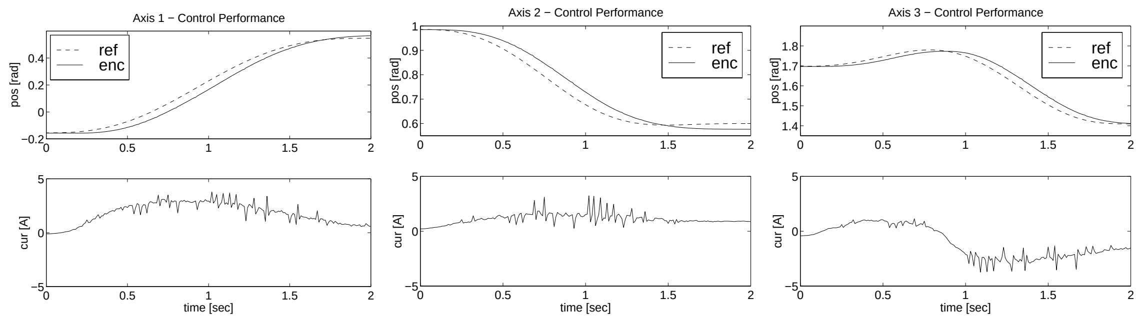

(a) Joint 1 performance

(b) Joint 2 performance

(c) Joint 3 performance

Figure 21: Experimental results for the quintic trajectory implemented on the SCORBOT ER VII.

List of Tables

Table I: SCORBOT ER VII estimated kinematic and dynamic parameters.

Link	$\theta[rad]$	$d[m]$	$a[m]$	$\alpha[rad]$
1	$\theta_1 = 0$	$d_1 = 0.3585$	$a_1 = 0.05$	$\alpha_1 = -\frac{\pi}{2}$
2	$\theta_2 = 0$	$d_2 = -0.037$	$a_2 = 0.30$	$\alpha_2 = 0$
3	$\theta_3 = 0$	$d_3 = 0.0$	$a_3 = 0.25$	$\alpha_3 = 0$
Link	Mass [kg]	$I_x[kgm^2]$	$I_y[kgm^2]$	$I_z[kgm^2]$
1	$m_1 = 0.0$	$I_{x1} = 0.00$	$I_{y1} = 0.05$	$I_{z1} = 0.0$
2	$m_2 = 6.6$	$I_{x2} = 0.10$	$I_{y2} = 0.60$	$I_{z2} = 0.6$
3	$m_3 = 4.2$	$I_{x3} = 0.02$	$I_{y3} = 0.20$	$I_{z3} = 0.3$

Table II: Imposed actuator torque and jerk bounds for the SCORBOT ER VII.

Torque limits $T[Nm]$	High jerk limits Example 1 $\dot{T}_1[Nm/sec]$	Medium jerk limits Example 2 $\dot{T}_2[Nm/sec]$	Low jerk limits Example 3 $\dot{T}_3[Nm/sec]$
$T_1 = 10$	$\dot{T}_{11} = 1000$	$\dot{T}_{12} = 100$	$\dot{T}_{13} = 10$
$T_2 = 10$	$\dot{T}_{21} = 1000$	$\dot{T}_{22} = 100$	$\dot{T}_{23} = 10$
$T_3 = 10$	$\dot{T}_{31} = 1000$	$\dot{T}_{32} = 100$	$\dot{T}_{33} = 10$

Table III: Simulated results for the PCTOM, SPCTOM, and quintic trajectories.

Trajectory	Jerk limits [Nm/sec]	Motion time [sec]	Maximum tracking error [cm]	RMS tracking error		
				joint 1 [^{o}]	joint 2 [^{o}]	joint 3 [^{o}]
PCTOM	∞	0.90	1.98	1.54	0.31	0.37
SPCTOM 1	1000	0.90	1.62	1.16	0.28	0.34
SPCTOM 2	100	0.74	1.40	1.12	0.26	0.33
SPCTOM 3	10	1.50	0.64	0.53	0.12	0.16
Quintic	7	2.00	0.51	0.42	0.10	0.12

Table IV: Experimental results for the PCTOM, SPCTOM, and quintic trajectories.

Trajectory	Jerk limits [Nm/sec]	Motion time [sec]	Maximum tracking error [cm]	RMS tracking error		
				joint 1 [^{o}]	joint 2 [^{o}]	joint 3 [^{o}]
PCTOM	∞	4.0	14.0	17.5	3.1	15.8
SPCTOM 1	1000	4.0	13.4	17.2	2.8	14.8
SPCTOM 2	100	4.0	12.5	15.9	2.6	14.8
SPCTOM 3	10	1.5	3.1	2.6	1.9	1.5
Quintic	7	2.0	2.5	2.3	1.8	1.4